

**CROSS-GRADIENT JOINT INVERSION OF 2D  
RESISTIVITY AND SEISMIC REFRACTION  
METHODS**

**NABILAH HUSNA BINTI ABDULLAH SANUSI**

**UNIVERSITI SAINS MALAYSIA**

**2021**

**CROSS-GRADIENT JOINT INVERSION OF 2D  
RESISTIVITY AND SEISMIC REFRACTION  
METHODS**

by

**NABILAH HUSNA BINTI ABDULLAH SANUSI**

**Thesis submitted in fulfilment of the requirements  
for the degree of  
Master of Science**

**October 2021**

## ACKNOWLEDGEMENT

I would like to express my gratitude to Allah SWT for giving me opportunity and help me endlessly in finishing this thesis. I would like to thank my supervisor Dr. Nur Azwin Binti Ismail for the continuous support of my master study. She consistently allowed this thesis to be my own work, but steered me in the right direction whenever she thought I needed it. My sincere thanks go to Geophysics lab staff Mr. Shahil Ahmad Khosaini and Mr. Zulkeflee Ismail for their time and energy assisting me in the projects. In my daily work I have been blessed with a helpful group of fellow friends in Geophysics course mate, Ms. Iffah Zalikha Roslan, Ms. Najmiah Rosli, Ms. Alyaa Nadirah Salleh, Ms. Nazirah Mahmud, Mr. Fakhru Hazwan Ahmad Fadzil, Mr. Taquiuddin Zakaria, Mr. Kiu Yap Chong, Mr. Muhammad Nazrin A Rahman, and Mr. Mark Jinmin. Special thanks to Ministry of Higher Education Malaysia for Fundamental Research Grant Scheme: FRGS/1/2018/STG09/USM/02/2.

Finally, I must express my very profound indebtedness to my parents, Abdullah Sanusi Ishak and Hayati Kidam, for providing me with unfailing support and continuous encouragement throughout my years of study and through the process of researching and writing this thesis. This accomplishment would not have been possible without their blessed and love. My appreciation also goes to my brothers; Muhammad Zharfan, Muhammad Nazmi, and Muhammad Zaim Nabil for their prayers, support and understanding during my study. Lastly, I want to thank all that not mention here especially my dearest friends for keep on give me strength to complete this master program. This thesis dedicated to all of you. Thank you.

## TABLE OF CONTENTS

<b>ACKNOWLEDGEMENT.....</b>	<b>ii</b>
<b>TABLE OF CONTENTS.....</b>	<b>iii</b>
<b>LIST OF TABLES.....</b>	<b>vi</b>
<b>LIST OF FIGURES.....</b>	<b>vii</b>
<b>LIST OF SYMBOLS.....</b>	<b>xiii</b>
<b>LIST OF ABBREVIATIONS.....</b>	<b>xv</b>
<b>LIST OF APPENDICES.....</b>	<b>xvi</b>
<b>ABSTRAK.....</b>	<b>xvii</b>
<b>ABSTRACT.....</b>	<b>xix</b>
<b>CHAPTER 1 INTRODUCTION.....</b>	<b>1</b>
1.1 Background.....	1
1.2 Problem statement.....	2
1.3 Objectives of the study.....	3
1.4 Scope of study.....	3
1.5 Significance of the study.....	4
1.6 Thesis layout.....	4
<b>CHAPTER 2 LITERATURE REVIEW.....</b>	<b>6</b>
2.1 Introduction.....	6
2.2 2D resistivity method.....	6
2.2.1 Resistivity of rocks and minerals.....	8
2.2.2 Type of electrode array.....	9
2.3 Seismic refraction method.....	11
2.3.1 Velocity of rocks and minerals.....	12
2.4 Forward modelling.....	13
2.5 Cross-gradient joint inversion method.....	15

2.5.1	Cross-gradient function.....	15
2.5.2	Joint inversion algorithm.....	17
2.6	Particle size distribution (PSD) analysis.....	19
2.7	X-ray diffraction (XRD) analysis.....	20
2.8	Previous research.....	21
2.9	Chapter summary.....	24
<b>CHAPTER 3 METHODOLOGY.....</b>		<b>26</b>
3.1	Introduction.....	26
3.2	Background of the study areas.....	28
3.3	Forward modelling.....	30
3.3.1	Model 1 .....	30
3.3.2	Model 2 .....	31
3.3.3	Model 3 .....	32
3.3.4	Model 4 .....	33
3.3.5	Model 5 .....	34
3.4	Data acquisition.....	35
3.4.1	2D resistivity survey .....	35
3.4.2	Seismic refraction survey .....	36
3.4.3	Bunker USM .....	37
3.4.4	Tapak Konvo USM .....	38
3.4.5	Guar Jentik .....	39
3.4.6	Indah Kembara .....	40
3.4.7	Bukit Chondong .....	41
3.5	Data processing.....	42
3.5.1	Individual inversion of 2D resistivity and seismic refraction data .....	42
3.5.2	Joint inversion with cross-gradient constraint .....	43

3.6	Geological analysis.....	44
3.6.1	Particle size distribution (PSD) analysis .....	44
3.6.2	X-ray diffraction (XRD) analysis .....	46
3.7	Chapter summary.....	47
<b>CHAPTER 4 RESULTS AND DISCUSSION.....</b>		<b>49</b>
4.1	Introduction.....	49
4.2	Synthetic models.....	50
4.2.1	Model 1.....	49
4.2.2	Model 2.....	54
4.2.3	Model 3.....	57
4.2.4	Model 4.....	60
4.2.5	Model 5.....	63
4.3	Field data.....	67
4.3.1	Bunker USM .....	67
4.3.2	Tapak Konvo USM .....	71
4.3.3	Guar Jentik .....	75
4.3.4	Indah Kembara .....	81
4.3.5	Bukit Chondong .....	87
4.4	Root mean square (RMS) value of the final models.....	95
4.4	Chapter summary.....	96
<b>CHAPTER 5 CONCLUSION.....</b>		<b>98</b>
5.1	Conclusion.....	98
5.2	Recommendations.....	100
<b>REFERENCES.....</b>		<b>101</b>
<b>APPENDICES</b>		
<b>LIST OF PUBLICATIONS</b>		

## LIST OF TABLES

	<b>Page</b>
Table 2.1 Resistivity ranges of rocks and minerals (Telford and Sheriff, 1984) .....	9
Table 2.2 Velocity of rocks and minerals (Telford & Sheriff, 1984).....	13
Table 3.1 The list of equipment as labelled in Figure 3.17 (b).....	45
Table 3.2 Summary of soil classification (after Santamarina et al., 2001).....	46
Table 4.1 Percentage of minerals composition of rock samples GJ1, GJ2, GJ3 and GJ4.....	77
Table 4.2 Summary of PSD analysis.....	83
Table 4.3 Percentage of minerals composition of rock samples BC1, BC2 and BC3.....	89
Table 4.4 Structural improvement in resistivity and seismic model after cross-gradient joint inversion for study area with lateral and vertical subsurface variation.....	94
Table 4.5 Root mean square (RMS) value of the final models for resistivity and seismic data from separate inversion and cross-gradient joint inversion. RMS values are recorded for each synthetic models and study areas.....	96

## LIST OF FIGURES

	<b>Page</b>
Figure 2.1	The arrangement of electrodes for a 2-D electrical survey and the sequence of measurements used to build up a pseudosection (Loke, 2004)..... 7
Figure 2.2	Common arrays used in resistivity surveys and their geometric factors (Loke, 1999)..... 10
Figure 2.3	The subsurface is subdivided into a large number of rectangular cells with specific resistivity values in each cell..... 14
Figure 2.4	The subsurface is subdivided into a large number of rectangular cells with specific velocity values in each cell..... 15
Figure 2.5	The arrows indicate the vector field of the (a) electrical and (b) seismic gradients. (c) The arrow in the yellow circle indicates structural similarity in that area. The yellow 'x' shows the area whereby the structure in the two models is dissimilar..... 17
Figure 3.1	Flow chart of the methodology..... 27
Figure 3.2	Geological map of Pulau Pinang (Ong, 1993)..... 29
Figure 3.3	Geological map of Perlis (Malaysian Mineral and Geoscience Department, 2007).....29
Figure 3.4	Synthetic (a) resistivity and (b) seismic model of Model 1 representing the lateral subsurface variation at Bunker USM.....31
Figure 3.5	Synthetic (a) resistivity and (b) seismic model of Model 2 representing the lateral subsurface variation at Tapak Konvo USM..... 32
Figure 3.6	Synthetic (a) resistivity and (b) seismic model of Model 3 representing the lateral subsurface variation at Tapak Konvo USM..... 33



Figure 3.7	Synthetic (a) resistivity and (b) seismic model of Model 4 representing the lateral subsurface variation at Tapak Konvo USM.....	34
Figure 3.8	Synthetic (a) resistivity and (b) seismic model of Model 5 representing the lateral subsurface variation at Tapak Konvo USM.....	35
Figure 3.9	Resistivity (blue arrow) and seismic (red arrow) survey line during field data acquisition.....	36
Figure 3.10	2D resistivity method equipment.....	37
Figure 3.11	Seismic refraction method equipment.....	37
Figure 3.12	Resistivity (blue arrow) and seismic survey (red arrow) line on Bunker USM.....	38
Figure 3.13	Resistivity (blue arrow) and seismic survey (red arrow) line across underground drain in Tapak Konvo USM.....	39
Figure 3.14	Resistivity (blue arrow) and seismic survey (red arrow) line on outcrop at Guar Jentik, Perlis.....	40
Figure 3.15	Resistivity (blue arrow) and seismic survey (red arrow) line at Indah Kembara.....	41
Figure 3.16	Resistivity (blue arrow) and seismic survey (red arrow) line on outcrop at Bukit Chondong.....	42
Figure 3.17	(a) A measuring cylinder of soil sample in a solution of Sodium Hexametaphosphate ( $\text{Na}_6[(\text{PO}_3)_6]$ ) and distilled water with hydrometer. (b) Stack of sieves was according to size.....	45
Figure 3.18	Instruments for XRD analysis have three major components: 1) X-ray source, 2) sample holder, and 3) detector.....	47
Figure 4.1	Separate inversion of (a) resistivity and (b) seismic model of Model 1. Cross-gradient joint inversion of (c) resistivity and (d) seismic model of Model 1.....	51
Figure 4.2	The arrows indicate the vector field of the (a) electrical resistivity and (b) seismic velocity gradients.....	52

Figure 4.3	Resistivity-velocity cross-plots derived from the (a) separate and (b) cross-gradient joint inversions of the resistivity and seismic data. 2D cross-plot model of resistivity and seismic refraction derived from (c) separate inversion and (d) cross-gradient joint inversion.....	53
Figure 4.4	Separate inversion of (a) resistivity and (b) seismic model of Model 2. Cross-gradient joint inversion of (c) resistivity and (d) seismic model of Model 2.....	55
Figure 4.5	The arrows indicate the vector field of the (a) electrical resistivity and (b) seismic velocity gradients.....	56
Figure 4.6	Resistivity-velocity cross-plots derived from the (a) separate and (b) cross-gradient joint inversions of the resistivity and seismic data. 2D cross-plot model of resistivity and seismic refraction derived from (c) separate inversion and (d) cross-gradient joint inversion.....	57
Figure 4.7	Separate inversion of (a) resistivity and (b) seismic model of Model 3. Cross-gradient joint inversion of (c) resistivity and (d) seismic model of Model 3. ....	58
Figure 4.8	The arrows indicate the vector field of the (a) electrical resistivity and (b) seismic velocity gradients.....	59
Figure 4.9	Resistivity-velocity cross-plots derived from the (a) separate and (b) cross-gradient joint inversions of the resistivity and seismic data. 2D cross-plot model of resistivity and seismic refraction derived from (c) separate inversion and (d) cross-gradient joint inversion.....	60
Figure 4.7	Separate inversion of (a) resistivity and (b) seismic model of Model 4. Cross-gradient joint inversion of (c) resistivity and (d) seismic model of Model 4. ....	62
Figure 4.8	The arrows indicate the vector field of the (a) electrical resistivity and (b) seismic velocity gradients.....	62

Figure 4.9	Resistivity-velocity cross-plots derived from the (a) separate and (b) cross-gradient joint inversions of the resistivity and seismic data. 2D cross-plot model of resistivity and seismic refraction derived from (c) separate inversion and (d) cross-gradient joint inversion.....	63
Figure 4.10	Separate inversion of (a) resistivity and (b) seismic model of Model 5. Cross-gradient joint inversion of (c) resistivity and (d) seismic model of Model 5.....	65
Figure 4.11	The arrows indicate the vector field of the (a) electrical resistivity and (b) seismic velocity gradients.....	65
Figure 4.12	Resistivity-velocity cross-plots derived from the (a) separate and (b) cross-gradient joint inversions of the resistivity and seismic data. 2D cross-plot model of resistivity and seismic refraction derived from (c) separate inversion and (d) cross-gradient joint inversion.....	66
Figure 4.13	Separate inversion of (a) resistivity and (b) seismic model of Bunker USM. Cross-gradient joint inversion of (c) resistivity and (d) seismic model of Bunker USM.....	69
Figure 4.14	The arrows indicate the vector field of the (a) electrical resistivity and (b) seismic velocity gradients.....	70
Figure 4.15	Resistivity-velocity cross-plots derived from the (a) separate and (b) cross-gradient joint inversions of the resistivity and seismic data. 2D cross-plot model of resistivity and seismic refraction derived from (c) separate inversion and (d) cross-gradient joint inversion.....	71
Figure 4.16	Separate inversion of (a) resistivity and (b) seismic model of Tapak konvo USM. Cross-gradient joint inversion of (c) resistivity and (d) seismic model Tapak konvo USM.....	73
Figure 4.17	The arrows indicate the vector field of the (a) electrical resistivity and (b) seismic velocity gradients.....	74

Figure 4.18	Resistivity-velocity cross-plots derived from the (a) separate and (b) cross-gradient joint inversions of the resistivity and seismic data. 2D cross-plot model of resistivity and seismic refraction derived from (c) separate inversion and (d) cross-gradient joint inversion.....	75
Figure 4.19	Outcrop of guar Jentik is at 27 m to 44.5 m on the resistivity line. Rock samples were taken for XRD analysis. GJ1, GJ2, and GJ4 were collected at Zone A, and GJ3 was collected at Zone B.....	76
Figure 4.20	XRD pattern of rock sample (a) GJ1 and (b) GJ3 at Guar Jentik.....	76
Figure 4.21	Separate inversion of (a) resistivity and (b) seismic model of Guar Jentik. Cross-gradient joint inversion of (c) resistivity and (d) seismic model of Guar Jentik. ....	79
Figure 4.22	The arrows indicate the vector field of the (a) electrical resistivity and (b) seismic velocity gradients.....	80
Figure 4.23	Resistivity-velocity cross-plots derived from the (a) separate and (b) cross-gradient joint inversions of the resistivity and seismic data. 2D cross-plot model of resistivity and seismic refraction derived from (c) separate inversion and (d) cross-gradient joint inversion.....	81
Figure 4.24	PSD graphs of soil samples at a depth of (a) 1.8 m and at (b) 2.8 m taken from Indah Kembara.....	82
Figure 4.25	Separate inversion of (a) resistivity and (b) seismic model of Indah Kembara. Cross-gradient joint inversion of (c) resistivity and (d) seismic model of Indah Kembara.....	85
Figure 4.26	The arrows indicate the vector field of the (a) electrical resistivity and (b) seismic velocity gradients.....	86
Figure 4.27	Resistivity-velocity cross-plots derived from the (a) separate and (b) joint inversions of the resistivity and seismic data. 2D cross-plot model of resistivity and seismic refraction derived from (c) separate inversion and (d) cross-gradient joint inversion.....	87

Figure 4.28	Outcrop of Bukit Chondong. Rock samples were taken for XRD analysis. BC 2 and BC 3 were collected at Zone A, and BC was collected at Zone B.....	88
Figure 4.29	XRD pattern of rock sample (a) GJ1 and (a) GJ3 taken at Guar Jentik.....	88
Figure 4.30	Separate inversion of (a) resistivity and (b) seismic model of Bukit Chondong. Cross-gradient joint inversion of (c) resistivity and (d) seismic model of Bukit Chondong.....	91
Figure 4.31	The arrows indicate the vector field of the (a) electrical resistivity and (b) seismic velocity gradients.....	92
Figure 4.32	Resistivity-velocity cross-plots derived from the (a) separate and (b) joint inversions of the resistivity and seismic data. 2D cross-plot model of resistivity and seismic refraction derived from (c) separate inversion and (d) cross-gradient joint inversion.....	93

## LIST OF SYMBOLS

C1, C2	Current electrode
P1, P2	Potential electrode
$V$	Potential difference
$I$	Current
$R$	Resistance
$A$	Ampere
$\rho$	Resistivity (rho)
$\Omega\text{m}$	Simplified unit of resistivity (ohm.metre)
$\text{m}$	Simplified unit for length (metre)
$\mu\text{m}$	Simplified unit for length (micrometre)
$\text{mm}$	Simplified unit for length (millimetre)
$\text{km/s}$	Simplified unit for speed (kilometre per second)
$\text{m/s}$	Simplified unit of velocity (meter per second)
$\text{g/ml}^3$	Simplified unit for density (gram per volume)
$\alpha$	Incidence ray
$\beta$	Refracted ray
$V_1, V_2$	Velocity of the first layer, velocity of the second layer
$V_p$	Velocity of P-wave
$\tau$	Cross-gradient function
$m_r, m_s$	Resistivity model, seismic model
$\nabla m_r, \nabla m_s$	Resistivity, seismic property gradient
$d_r, d_s$	Observed resistivity data, observed travel time data
$F_r, F_s$	Forward modelling function for resistivity, forward modelling function for seismic

$C_{dr}, C_{ds}$	Covariance matrix of resistivity, covariance matrix of seismic velocity data
$w_r, w_s$	Weighting factors for resistivity data, weighting factors for the seismic data
$\lambda_r, \lambda_s$	Regularization weight for resistivity model, regularization weight for velocity model
D	First difference flatness matrix operator
$m_{(r, ap)}, m_{(s, ap)}$	A priori resistivity model, a priori seismic model
$\alpha_r, \alpha_s$	Weighing factors for $m_{(r, ap)}$ , weighing factors for $m_{(s, ap)}$
k	Iteration number
A	Jacobian matrix
$\Delta d$	Difference between observed data and modelled data at current iterate
$\psi$	Objective function
n	(An integer) order of diffraction
$\lambda$	Wavelength of the incident X-rays
d	Lattice spacing
$\theta$	Angle of incidence
%	Percent
$Na_6[(PO_3)_6]$	Sodium Hexametaphosphate
$>, \geq$	Greater than, greater than or equal to
$<, \leq$	Lesser than, lesser than or equal to
w	Moisture content

## LIST OF ABBREVIATIONS

2D	Two-dimensional
PSD	Particle size distribution
XRD	X-ray diffraction
USM	Universiti Sains Malaysia
BS	British Standard
RMS	Root mean square
GJ	Guar Jentik
BC	Bukit Chondong



## LIST OF APPENDICES

Appendix A	Recorded seismogram for Model 1
Appendix B	Recorded seismogram for Model 2
Appendix C	Recorded seismogram for Model 3
Appendix D	Recorded seismogram for Model 4 and 5
Appendix E	XRD pattern of the rock sample at Guar Jentik: GJ1, GJ2, GJ3 and GJ4
Appendix F	PSD analysis graph for soil sample of the study area in Indah Kembara at a depth of 1.8 m, 2.8m, and 3.6 m
Appendix G	XRD pattern of the rock sample at Bukit Chondong: BC1, BC2, and BC3

# **SONGSANGAN BERSAMA KECERUNAN SILANG TERHADAP KAEDAH KEBERINTANGAN 2D DAN PEMBIASAN SEISMIK**

## **ABSTRAK**

Penyiasatan permukaan bawah tanah biasanya melibatkan kaedah geofizik seperti kaedah keberintangan 2D dan pembiasan seismik. Setiap kaedah bergantung pada parameter fizikal yang berbeza dan mempunyai kepekaan yang berbeza pada struktur subpermukaan. Dalam kajian ini, songsangan bersama kecerunan silang telah dilakukan untuk memetakan dan menambah baik pencirian imej variasi lateral dan menegak subpermukaan. Idea asas pendekatan ini adalah untuk mencapai model geologi seragam yang memenuhi syarat kedua-dua set data dengan menggunakan kekangan kecerunan silang. Kaedah ini telah dijalankan pada lima model sintetik dengan variasi subpermukaan secara lateral (Model 1, Model 2, dan Model 3) dan variasi subpermukaan secara menegak (Model 4 dan Model 5). Kemudian, kaedah ini telah diterapkan ke kawasan kajian dengan variasi subpermukaan secara lateral (Bunker USM, Tapak Konvo USM, dan Guar Jentik) dan variasi subpermukaan secara menegak (Indah Kembara dan Bukit Chondong). Analisis taburan saiz partikel (PSD) dan pembelauan sinar-X (XRD) juga telah dilakukan pada sampel tanah dan batu di Indah Kembara, Guar Jentik, dan Bukit Chondong. Songsangan bersama kekangan kecerunan silang model seismik dengan variasi subpermukaan secara lateral menunjukkan struktur anomali yang bertambah baik. Sementara itu, kedua-dua model songsangan berasingan dengan variasi subpermukaan secara menegak sudah pun menunjukkan persamaan struktur, oleh itu tidak ada perubahan pada kedua-dua model songsangan bersama kekangan kecerunan silang. Variasi subpermukaan secara lateral, seperti Bunker USM dan Tapak Konvo USM

menunjukkan peningkatan dari segi struktur bunker ( $<40 \Omega_m$ , 1.4 - 1.6 km/s) dan longkang ( $<50 \Omega_m$ ,  $<0.9$  km/s) pada model songsangan bersama seismik. Model songsangan bersama keberintangan dan seismik meleraikan struktur secara menegak batu pasir ( $> 120 \Omega_m$ ,  $> 2.5$  km/s) dan batu lumpur ( $<120 \Omega_m$ ,  $<2.5$  km/s) pada sinkapan Guar Jentik. Variasi subpermukaan secara menegak di Indah Kembara menunjukkan peningkatan struktur lapisan subpermukaan pasir lumpur ( $>100 \Omega_m$ ,  $<0.7$  km/s) dan tanah liat ( $<100 \Omega_m$ ,  $>0.7$  km/s) pada model songsangan bersama seismik. Persempadanan batu pasir ( $>1000 \Omega_m$ ,  $>3.7$  km/s) tertanam di antara batu lumpur ( $<1000 \Omega_m$ ,  $<3.7$  km/s) di Bukit Chondong telah menunjukkan peningkatan dari segi struktur pada songsangan bersama model keberintangan dan seismik. Analisis plot silang yang berasal dari kecerunan silang songsangan bersama mempunyai data yang kurang terserak yang membentuk kelompok yang menentukan kehadiran sempadan geologi di subpermukaan. Nilai punca kuasa dua (RMS) untuk songsangan berasingan di kawasan kajian adalah  $RMS_r = 0.06 - 0.36$ ;  $RMS_s = 5.27 - 14.3$ . Untuk songsangan bersama kekangan kecerunan silang, nilai RMS adalah  $RMS_r = 0.095 - 0.87$ ;  $RMS_s = 5.5 - 16.4$ . Walau bagaimanapun, mendapatkan model yang seragam adalah lebih penting dalam proses penafsiran model keberintangan dan seismik. Oleh itu, kaedah songsangan bersama kecerunan silang telah berjaya diterapkan pada variasi subpermukaan secara lateral dan menegak untuk memetakan dan meningkatkan imej pencirian subpermukaan sambil mengenal pasti sifatnya.

# **CROSS-GRADIENT JOINT INVERSION OF 2D RESISTIVITY AND SEISMIC REFRACTION METHODS**

## **ABSTRACT**

Subsurface investigation commonly involved geophysical methods such as 2D resistivity and seismic refraction methods. Each methods are dependent on different physical parameters and has different sensitivity on subsurface structure. In this study, joint inversion with a cross-gradient constraint method was conducted to map and improved image characterization of lateral and vertical subsurface variation. The basic idea of this approach was to achieve a unified geological model which satisfies both data sets using cross-gradient constraint. This method was conducted on five synthetic models with lateral subsurface variation (Model 1, Model 2, and Model 3) and vertical subsurface variation (Model 4 and Model 5) as preliminary studies. Then, this method was applied to the study areas with lateral subsurface variation (Bunker USM, Tapak Konvo USM, and Guar Jentik) and vertical subsurface variation (Indah Kembara and Bukit Chondong). Particle size distribution (PSD) and X-ray diffraction (XRD) analysis were also conducted on soil and rock samples at Indah Kembara, Guar Jentik, and Bukit Chondong. Cross-gradient joint inversion of seismic model with lateral subsurface variation shows structural improvement of the anomaly. Meanwhile, separate inversion models with vertical subsurface variation already show structural similarities, hence no changes in both cross-gradient joint inversion models. Lateral subsurface variation such as Bunker USM and Tapak Konvo USM shows a structural improvement of the bunker ( $<40 \Omega\text{m}$ , 1.4 - 1.6 km/s) and drain ( $< 50 \Omega\text{m}$ ,  $<0.9$  km/s) in joint inversion of seismic models. Joint inversion of resistivity and seismic model resolved the vertical

structure of sandstone ( $>120 \Omega\text{m}$ ,  $>2.5 \text{ km/s}$ ) and mudstone ( $<120 \Omega\text{m}$ ,  $<2.5 \text{ km/s}$ ) in Guar Jentik. Vertical subsurface variation at Indah Kembara shows an improved subsurface layers of silty sand ( $>100 \Omega\text{m}$ ,  $<0.7 \text{ km/s}$ ) and silty clay ( $<100 \Omega\text{m}$ ,  $>0.7 \text{ km/s}$ ) in joint inversion of seismic model. The delineation of sandstone ( $>1000 \Omega\text{m}$ ,  $>3.7 \text{ km/s}$ ) interbedded with mudstone ( $<1000 \Omega\text{m}$ ,  $<3.7 \text{ km/s}$ ) in Bukit Chondong also has improved in joint inversion of resistivity and seismic models. Cross-plot analysis derived from cross-gradient joint inversion had less dispersed data that formed a cluster defining a presence of geological boundary in the subsurface. The root mean square (RMS) value for separate inversion at study areas are  $\text{RMS}_r = 0.06 - 0.36$ ;  $\text{RMS}_s = 5.27 - 14.3$ . For cross-gradient joint inversion, the RMS value are  $\text{RMS}_r = 0.095 - 0.87$ ;  $\text{RMS}_s = 5.5 - 16.4$ . Despite that, achieving a unified model is more important in the resistivity and seismic model interpretation processes. Therefore, cross-gradient joint inversion method was successfully applied on lateral and vertical subsurface variation.

# CHAPTER 1

## INTRODUCTION

### 1.1 Background

Subsurface is a term that refers to the strata or layers of soil or rock deposits that exist beneath the Earth's surface. Earth processes and geological activities result in a heterogeneous and complex subsurface that exhibits lateral and vertical variation. Lateral subsurface variation refers to vertical or nearly vertical contrast boundaries that cut through or across strata, such as dykes, faults, or fractures, whereas vertical subsurface variation refers to horizontal contrast boundaries between strata, such as sediments deposited as flat-lying layers overlying or underlying different strata. Groundwater, overburden, and bedrock are just a few examples. Because the subsurface is composed of lateral and vertical variation, interpretations based on a single type of geophysical data are less favorable (Ali et al., 2017; Anuar et al., 2017a; Yusoh et al., 2018).

Geophysical methods are frequently used for subsurface investigation because they can provide data quickly and with high accuracy while being environmentally friendly. 2D resistivity and seismic refraction are the two common geophysical methods. The 2D resistivity method is capable of subsurface mapping and providing information about the subsurface (Asry et al., 2012). On the other hand, seismic refraction method can be used to determine shallow subsurface conditions or to estimate the thickness of stratified soil and rock layers, which provides information about subsurface characteristics (Anomohanran, 2013). However, the complex subsurface with vertical and lateral variations will influence the current flow from 2D resistivity and the acoustic wave propagation from seismic refraction survey. To address this issue, Gallardo and Meju (2003) pioneered the use

of a cross-gradient function as a constraint in the non-linear least-square problem to perform a joint inversion of resistivity and seismic data. This joint inversion method enhances interpretation by providing structurally similar resistivity and seismic models.

This study used 2D resistivity and seismic refraction methods to map the subsurface with lateral and vertical variation in five study areas. The variations in the subsurface included geological structures and man-made structures. Apart from separate inversion, this study also utilized joint inversion with a cross-gradient constraint method to generate their respective resistivity and seismic inversion models. Besides that, particle size distribution (PSD) and X-ray diffraction (XRD) analyses were conducted to assist in classifying the soil and rock types in the study area.

## **1.2 Problem statement**

2D resistivity method is more sensitive in resolving lateral velocity changes compared to seismic refraction method. On the other hand, seismic refraction is a more sensitive method for detecting changes in vertical property. It is frequently difficult to satisfy both resistivity and seismic models due to the fact that the data sets were dependent on different physical parameters. Additionally, because inverse problems are non-unique, there will be multiple solutions that adequately explain the observed data (Meju, 1994). One method for reducing non-uniqueness in inverse problems is to jointly invert resistivity and seismic data simultaneously using the cross-gradient constraint. Joint inversion can alleviate the limitations and ambiguity associated with individual data and result in a more easily interpretable model (Santos et al., 2006), as the cross-gradient function evaluates the structural similarity between two models (Gallardo and Meju, 2004).

### **1.3 Objectives of the study**

The purposes of this study are:

- i. To map the lateral and vertical extend of subsurface geological structure in study area.
- ii. To improve the image characterization of the subsurface using cross-gradient joint inversion method.
- iii. To identify the properties of subsurface in study area using geological analyses.

### **1.4 Scope of study**

In this study, 2D resistivity method is used with seismic refraction method to map the lateral and vertical subsurface. The 2D resistivity line was run parallel to the seismic refraction line to ensure that both methods provided information at the same location. This study is divided into two sections: forward modeling and field data collection. Forward modeling created five synthetic models that are used as references and guidelines for the study area. The study areas are located inside of Universiti Sains Malaysia (USM), Pulau Pinang and Perlis. Initially, 2D resistivity and seismic refraction data are inverted separately. Following that, cross-gradient joint inversion of 2D resistivity and seismic refraction data is used to construct their respective resistivity and seismic models with structure improvement. Separate inversion results are compared to the cross-gradient joint inversion result. At the same time, PSD and XRD analyses are conducted to help identifying the type of soil and rocks in the study area.



## **1.5 Significance of the study**

The purpose of this study is to demonstrate the efficacy of the cross-gradient joint inversion method for mapping lateral and vertical subsurface variation. The fundamental idea behind this approach is to generate a unified geological model that accounted for both 2D resistivity and seismic refraction data. Traditionally, multi-parameter geophysical methods are performed by inverting or processing each data set independently and comparing the resulting inversion models. This approach may introduce interpretive uncertainty, as each method has different parameters and possessed different sensitivity and limitations. To satisfy the various parameters, a joint inversion method based on cross-gradient constraint is used to enforce structural similarity between the resistivity and seismic models via regularization terms derived from the cross-product of their gradients. The cross-gradient joint inversion method enables the construction of structurally similar resistivity and seismic inversion models that were previously impossible to construct using separate inversion methods.

## **1.6 Thesis layout**

The thesis chapters are organized as follows:

Chapter 2 is divided into two sections. The first section discussed forward modeling theory, 2D resistivity, seismic refraction, joint inversion with cross gradient constraint, PSD analysis, and XRD analysis. The second section of this chapter discussed the previous study in detail.

Chapter 3 discussed the study areas' location and geology, and research methodology. The study is divided into two sections: forward modeling and field data collection. This chapter also discussed the data collection procedures, the equipment used in the study, and the data processing.

Chapter 4 reported the research and interpretations from this study. The findings are divided into two categories: forward modeling and field data. Indah Kembara, Guar Jentik, Bukit Chondong, Bunker USM, and Tapak Konvo USM are among the locations where field data are collected. The results in Indah Kembara, Guar Jentik, and Bukit Chondong are interpreted using additional PSD and XRD data. Additionally, cross-plots between resistivity and velocity are plotted for both separate inversion and joint inversion models.

Finally, chapter 5 summarized the application of cross-gradient joint inversion of 2D resistivity and seismic refraction methods for mapping subsurface structures with lateral and vertical variation. Several recommendations for future research are included.

## CHAPTER 2

### LITERATURE REVIEW

#### 2.1 Introduction

This chapter discussed the theory of 2D resistivity, seismic refraction, forward modelling, joint inversion with cross-gradient constraint, particle size distribution (PSD) analysis, and X-ray diffraction (XRD) analysis. Besides that, this chapter contains references to previous studies that are relevant to the research.

#### 2.2 2D resistivity method

The 2D resistivity method is one of the oldest and most widely used geophysical exploration techniques (Reynolds, 2011). It is used to image subsurface structures using electrical resistivity measurements at the surface through electrodes. The current is injected through two current electrodes, C1 and C2, while potential difference ( $\Delta V$ ) at two potential electrodes, P1 and P2 are measured. Resistivity survey is based on Ohm's Law, which describes the behavior of current flow in the ground (Loke, 2004). The equation for Ohm's law in vector form is given by (Equation 2.1),

$$V = IR \quad 2.1$$

where,

V = potential difference (V)

I = current (A)

R = resistance ( $\Omega$ )

The calculated resistivity values are not the true resistivity of the subsurface but an apparent resistivity value. The apparent resistivity values can estimate the earth's true resistivity and locate their boundaries below the earth's surface layer. To determine the true subsurface resistivity from the apparent resistivity values, an "inversion" problem are used (Loke, 1999). A pseudosection contouring is built up based on the sequence of measurements to present the apparent resistivity values that will give an approximate picture of subsurface resistivity distribution. It is an appropriate technique for complex geology areas to provide detailed subsurface information (Asry et al., 2012). The resistivity model is assumed to differ vertically and laterally along the survey line but constant in the direction perpendicular to the survey line. This method is usually carried out using electrodes with constant spacing between adjacent electrodes and are connected to a multi-core cable. The multi-core cable is attached to an electronic switching unit connected to a laptop computer (Figure 2.1).

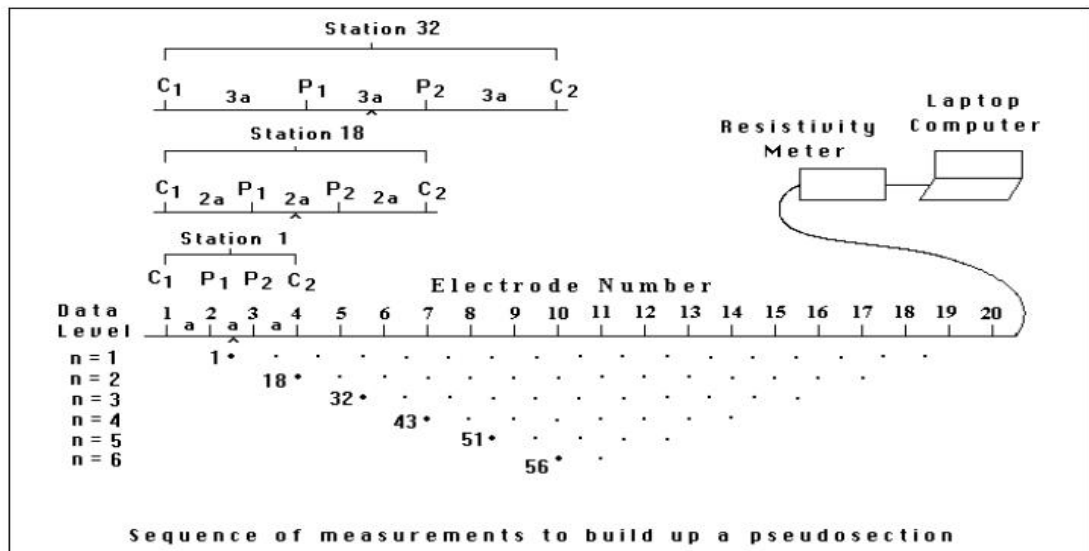


Figure 2.1 The arrangement of electrodes for a 2-D electrical survey and the sequence of measurements used to build up a pseudosection (Loke, 2004)

This method has been applied in a variety of fields, including environmental engineering, mineral exploration, archaeology, and hydrology (Rosli et al., 2018; Giang et al., 2013; Abidin et al., 2011; Chambers et al., 2006). It is used to image the subsurface, discovering geological structures such as faults, contacts, and fractures (Anuar et al., 2018; Saetang et al., 2014). Besides that, it can assist to develop a subsurface soil profile to define the groundwater zone and determining the unsaturated and saturated layers (Ashraf et al., 2018; Asry et al., 2012).

### **2.2.1 Resistivity of rocks and minerals**

Resistivity ( $\rho$ ) or also defined as resistance per unit length and per unit of cross sectional area in Ohm metre ( $\Omega\text{m}$ ) unit, is determined by the ability of rock, soil, and groundwater to pass through electrical current (Loke, 1999). Table 2.1 shows the approximate resistivity ranges of rocks and minerals. Geological parameters such as grain size, porosity, fluid content, and density influenced the resistance of different types of rocks, soil, and minerals. The presence of fractures and the percentage of fractures filled with groundwater determine the resistivity of igneous and metamorphic rocks. If the rock is dry, its resistivity value will be high, and vice versa. Due to its high porosity and water content, sedimentary rock can have low resistivity values. Coarse-grained soil has a higher permeability, which allows for easy percolation of water and results in a high resistivity value (Abidin et al., 2015, 2017). The resistivity of unconsolidated sediments is also dependent on their clay content. Clayey soils, on average, have a lower resistivity than sandy soils.

Table 2.1 Resistivity ranges of rocks and minerals (Telford and Sheriff, 1984)

Materials	Resistivity ( $\Omega\text{m}$ )
Igneous/Metamorphic	
Granite	$5 \times 10^3 - 10^8$
Weathered granite	$1 - 10^2$
Basalt	$10^3 - 10^6$
Quartz	$10^3 - 2 \times 10^6$
Marble	$10^2 - 2.5 \times 10^8$
Schist	$20 - 10^4$
Sediments	
Sandstone	$8 - 4 \times 10^3$
Conglomerate	$2 \times 10^3 - 10^4$
Shale	$20 - 2 \times 10^3$
Limestone	$50 - 4 \times 10^2$
Unconsolidated sediment	
Clay	$1 - 100$
Alluvium	$10 - 800$
Marl	$1 - 70$
Clay (wet)	$20$
Groundwater	
Freshwater	$10 - 100$
Saltwater	$0.2$

### 2.2.2 Type of electrode arrays

Wenner, Wenner-Schlumberger, pole-dipole, and dipole-dipole arrays are the most frequently used arrays for 2D resistivity method. The configuration of each array is shown in Figure 2.2. Different type of arrays used can affect the imaging efficiency because it depends on sensitivity to the target of interest, level of noise, and type of structure to be mapped (Loke, 2004). It is important to choose a suitable electrode array that produce good results with high resolution and reliable subsurface image. Characteristics of an array that should be considered are the depth of investigation, the sensitivity of the array to vertical and horizontal changes in the subsurface resistivity, the horizontal data coverage, and the signal strength (Loke, 2004). For this study, a pole-dipole array was chosen because it has good horizontal coverage, good signal strength, and can give deeper coverage of subsurface compared to the other configurations (Loke, 2004).

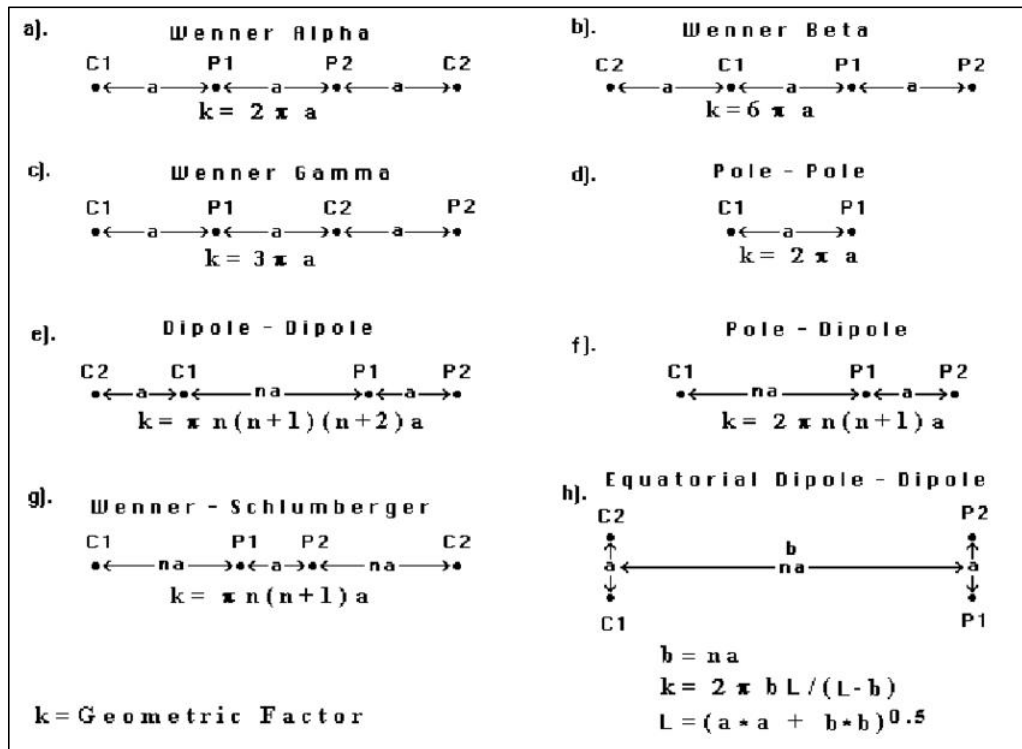


Figure 2.2 Common arrays used in resistivity surveys and their geometric factors (Loke, 1999)

Based on Figure 2.2, the pole-dipole array uses two potential electrodes, P1 and P2, and two current electrodes, C1 and C2. P1 and P2 are separated with spacing  $a$ , which moves along the line for  $n$  spacing from current electrode C1. This array requires a remote electrode, C2, and must be planted far away from the survey line perpendicularly. It has multi-electrode resistivity meter systems with a relatively small number of nodes, which gives good data coverage. The spatial resolution and the penetration depth of an electrode array are related to the basic spacing and the maximum separation of electrodes which are determined by the geological models and the noise contamination levels. The pole-dipole array exhibits a low signal-to-noise ratio. Despite its moderate anomaly effects and low signal-to-noise ratio, a pole-dipole array can produce images with a higher spatial resolution than other arrays (Dahlin and Zhou, 2004; Martorana et al., 2017). It also has a deeper depth of investigation compared to other types of array.

### 2.3 Seismic refraction method

Seismic refraction method is frequently used to determine the depth to bedrock, water table, or other seismic velocity boundaries. A seismic wave is generated at the ground surface by an impulsive source and traveled through the earth. When the wavefront reached a layer of higher velocity, a portion of the energy will be critically refracted and will travel along with the refractor at the refractor's velocity. The energy emitted by the propagating head wave exit the refractor and is reflected back to the surface. Geophone will detect its arrival and will be recorded on a seismograph. The ratio of velocities in the two materials affected the angle of refraction according to Snell's law of light and the phenomenon of critical incidence (Equation 2.2 and 2.3),

$$\frac{\sin \alpha}{\sin \beta} = \frac{V_1}{V_2} \quad 2.2$$

Critical incidence occurs when  $\beta = 90^\circ$ . So,

$$\sin \alpha = \frac{V_1}{V_2} \quad 2.3$$

where;

$\alpha$  = incidence ray

$\beta$  = refracted ray

$V_1$  = velocity of the first layer (m/s)

$V_2$  = velocity of the second layer (m/s)



The time for the first arrival signals of the data are pick to generate a travel time–distance curve and produce a 2D seismic velocity depth profiles. Parameters such as travel time data and distances of geophone are used for calculation to obtain the  $V_p$  values and the thickness of each layer. The parameters will go through seismic inversion process to generate seismic inversion profiles.

Seismic refraction has become one of the most common methods used in the subsurface investigation and has been implemented to delineate geological fault (Saetang et al., 2014; Nyabeze et al., 2018; Anuar et al., 2017a), finding groundwater (Moustafa et al., 2013, Ashraf et al., 2018; Azhar et al., 2019), delineating buried bunker (Bery et al.,2018) and inferring tunnel locations (Riddle et al., 2010; Ding and Jiang, 2016). This method is able to determine the thickness of stratified layers of soil and rock that will contribute information about subsurface characteristics (Anomohanran, 2013).

### **2.3.1 Velocity of rocks and minerals**

The velocity of rocks and minerals depend on the elastic moduli and density, which also depend on the properties of rock and minerals. Therefore, it is necessary to have some knowledge such as mineral content, size of the grain, density, and fluid content in order to interpret seismic results. Typical values of the seismic velocity,  $V_p$  of some rocks and minerals are listed in Table 2.2. The measured value of velocity is used to solve several problems regarding the depth variations in seismic velocities, porosity, and permeability.

There are underlying principles in the velocity of rock and soil. Unsaturated and unconsolidated sediments have lower velocity values than saturated and consolidated sediment. For rock, the velocity value of weathered rocks is lower

than unweathered rocks. Velocity value is also lower for some metamorphic and igneous rock compared to sedimentary rock because of compaction and lithification. Fracture rocks that are either filled with liquid or gas have lower velocity values than unfractured rocks because it reduces the stiffness of rocks, thus lower seismic wave speed.

Table 2.2 Velocity of rocks and minerals (Telford & Sheriff, 1984)

Materials	Seismic velocity (m/s)
Igneous/Metamorphic	
Granite	4580 - 5800
Weathered granite	305 - 610
Basalt	5400 - 6400
Sedimentary	
Sandstone	1830 - 3970
Shale	2750 - 4270
Limestone	2140 - 6100
Unconsolidated sediment	
Clay	915 - 2750
Alluvium	500 - 2000
Groundwater	
Freshwater	1430-1680
Saltwater	1460-1530

## 2.4 Forward modelling

Forward modeling is a process of calculating a response from a physical property model. This method constructs a synthetic model to simulate the geological subsurface of a study area. This helps to see whether the apparent value is agreed with the measured values. In this study, forward modelling is used to construct synthetic resistivity and seismic models based on the study areas.

The purpose of resistivity forward modelling is to calculate the apparent resistivity that would be measured by a survey for the model produced by the inversion routine. Finite-element and finite-difference methods are more suitable for engineering and environmental surveys because the subsurface can have an arbitrary

resistivity distribution. This method is based on Dey and Morrison (1979a), but Loke (2001) modified it to correct for a minor inconsistency in the Dey and Morrison discretization by area method. The subsurface is subdivided into a large number of rectangular cells, as shown in Figure 2.3. The subsurface resistivity distribution of each cell is specified.

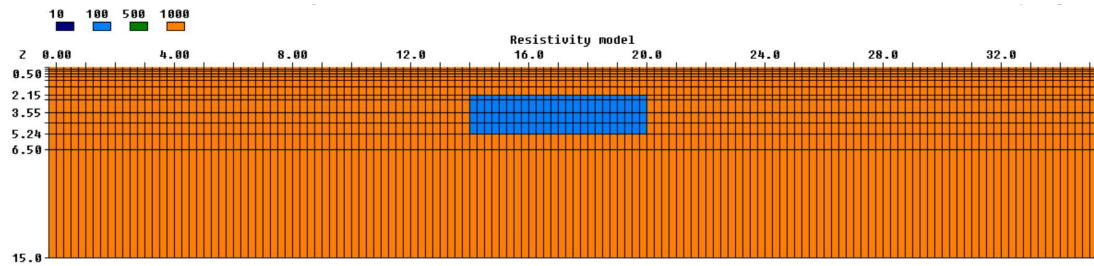


Figure 2.3 The subsurface is subdivided into a large number of rectangular cells with specific resistivity values in each cell

For seismic model, forward modelling method is conducted to simulate wave propagation in the earth for a geological model, presumed the structure of given subsurface (Carcione et al., 2002). It is possible to generate a seismic response, which should be similar to stacked sections resulting from the processing of real seismic data. Models can be 1D, 2D, or 3D and consist of depth horizons and associated P-wave velocity, S-wave velocity, and density. Seismic forward modeling can be done by ray-tracing approaches. The subsurface is subdivided by cells with specific velocity value (Figure 2.4), and seismic ray goes through the cells with specified depth. Rays will hit the target and will reflect back to the receivers.

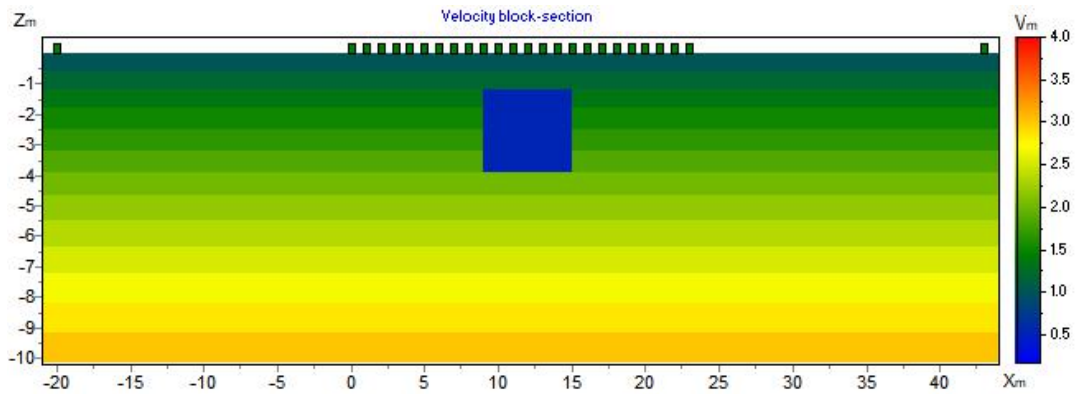


Figure 2.4 The subsurface is subdivided into a large number of rectangular cells with specific velocity values in each cell

## 2.5 Cross-gradient joint inversion method

In geophysics, the inversion process is involved in converting measured data sets into reasonable models portraying physical property distribution in the ground. It is the opposite of forward modelling. In most cases, inverse problems are often affected by errors in observational data, limitations in the survey area, and simplification of an underground model (Kabanikhin, 2008). The non-uniqueness inherent in the inversion method often results in several different models, and this could decrease the accuracy in interpretation of data (Meju, 1994). Therefore, in this study, joint inversion method with cross-gradient constraint is chosen to overcome this limitation and to reduce the multi-solution of inversion.

### 2.5.1 Cross-gradient function

The principle of cross-gradient constrains is to progressively seek a degree of structural similarities between the images constructed from the inversion model of resistivity and seismic data. The physical properties utilized by different geophysical methods such as 2D resistivity and seismic refraction methods are expected to produce images with a degree of structural similarity (Haber and Oldenburg, 1997). The most crucial part of the joint inversion is to link the model parameters in seeking

structural similarities where cross-gradients function is implemented such given in Equation 2.4 (Gallardo and Meju 2003);

$$\tau(m_r, m_s) = \nabla m_r \times \nabla m_s = \nabla m_r \times \nabla m_s \sin \theta \quad 2.4$$

where;

$\tau$  = cross-gradient function

$m_r$  = resistivity model

$m_s$  = seismic model

$\nabla m_r$  = resistivity property gradient

$\nabla m_s$  = seismic property gradient

$\theta$  = angle of resistivity and seismic property gradient

Equation 2.4 can be included in the inversion objective function as a constraint, as discussed in the upcoming section (Section 2.5.2). This approach has been implemented with success in several fields, such as near-surface geophysics (Gallardo and Meju, 2003; Doetsch et al., 2015) and oil and gas prospecting (Meju et al., 2019).

Figure 2.5 explains the concept of cross-gradient constraint to find the structural similarity between 2D resistivity and seismic refraction. According to Gallardo and Meju (2003), the structural similarities between 2D resistivity and seismic refraction images are related to the distribution of electrical and seismic gradient in each models. These attributes can be mathematically represented by the vector field of the electrical and seismic gradients. The resistivity and seismic models are identified as structurally similar if the cross-gradient function is equal to zero, where vector field of electrical and seismic gradients must be in the same or opposite

direction (parallel to each other) regardless of amplitudes. In a geological context, this suggests that both methods must identify the existence of boundaries in a common orientation of the changing physical properties. It should be clarified that the implemented cross-gradient constraint is used for geological structural control but does not impose the two models to conform if not validated by any of the data sets.

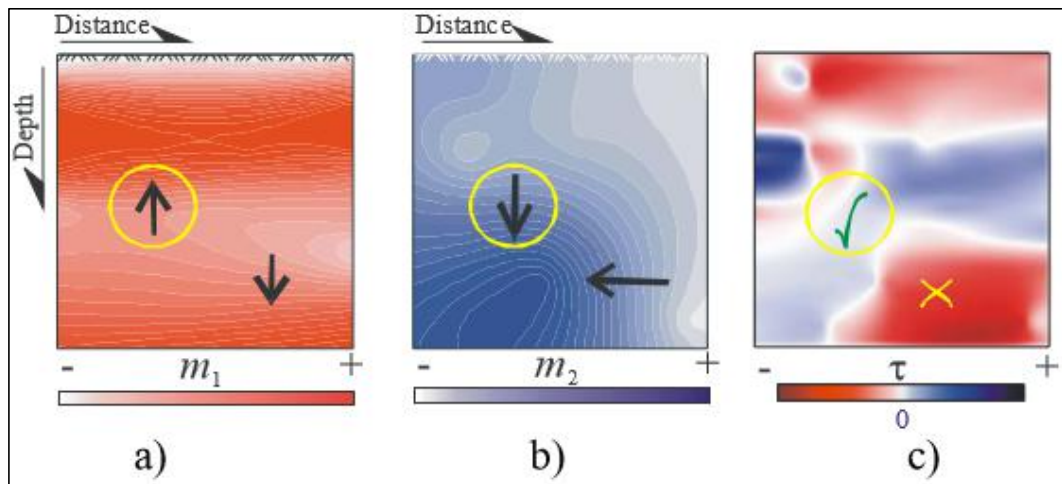


Figure 2.5 The arrows indicate the vector field of the (a) electrical and (b) seismic gradients. (c) The arrow in the yellow circle indicates structural similarity in that area. The yellow 'x' shows the area whereby the structure in the two models is dissimilar (after Gallardo et al., 2005)

## 2.5.2 Joint inversion algorithm

Joint inversion is used to integrate varying geophysical data and show a more consistent and reliable result for subsurface models and interpretations when compared to individual geophysical data inversion (Gallardo and Meju, 2003; Saunders et al., 2005; Gallardo and Meju, 2007; Gallardo et al., 2012; Doetsch et al., 2015; Feng et al., 2018). The subsurface is discretized by 2D rectangular cells characterized by physical properties of resistivity and seismic velocity. The objective function,  $\psi$  for the joint inversion, is shown in Equation 2.5, and it is similar to Meju et al. (2019),

$$\begin{aligned}
\psi(m_r, m_s) = & w_r \cdot C_{dr}^{-1} \|d_r - F_r(m_r)\|^2 + w_s \cdot C_{ds}^{-1} \|d_s - F_s(m_s)\|^2 \\
& + \lambda_r \|Dm_r\|^2 + \lambda_s \|Dm_s\|^2 + \tau \|\nabla m_r \times \nabla m_s\|^2 \\
& + \alpha_r \|m_r - m_{r,ap}\|^2 + \alpha_s \|m_s - m_{s,ap}\|^2
\end{aligned} \tag{2.5}$$

where;

$d_r, d_s$  = observed resistivity data, observed travel time data

$m_r, m_s$  = resistivity model, velocity model

$F_r, F_s$  = forward modelling function for resistivity, forward modelling function for seismic

$C_{dr}, C_{ds}$  = covariance matrix of resistivity, covariance matrix of seismic velocity data

$w_r, w_s$  = weighting factors for resistivity data, weighting factors for the seismic data

$\lambda_r, \lambda_s$  = regularization weight for resistivity model, regularization weight for velocity model

$D$  = first difference flatness matrix operator

$\tau$  = cross-gradient weight

$m_{(r, ap)}, m_{(s, ap)}$  = a priori resistivity model, a priori seismic model

$\alpha_r, \alpha_s$  = weighing factors for  $m_{(r, ap)}$ , weighing factors for  $m_{(s, ap)}$

Based on Equation 2.5, the fifth term contains the cross-gradients values as shown previously in Equation 2.4 and can be calculated using finite difference approximation as in Meju et al. (2019). The objective function is minimized using the iterative Gauss-Newton approach to achieve optimum model solutions. The sequence of the model update is given by (Equation 2.6);

$$m^k = m^{k-1} + \alpha(A^T A)^{-1} A^T \Delta d \tag{2.6}$$

where;

$m$  = model parameter

$k$  = iteration number

$\alpha$  = step length

$A$  = Jacobian matrix which is derivative of Equation 2.6 with respect to  $m$

$T$  = matrix transpose

$\Delta d$  = difference between observed data and modelled data at current iterate  $k-1$

The optimal step length,  $\alpha$ , is determined through line search to ensure that the resulting objective function,  $\psi$  is lower than the previous iterate. This approach seeks to optimize the structurally similar resistivity and velocity models but still explains the observed data reasonably well.

## **2.6 Particle size distribution (PSD) analysis**

The particle size distribution (PSD) method is used to classify the dry mass of soil into specified particle-size ranges. It can classify soils according to the percentage of gravel, sand, silt, and clay in the soil, as indicated by the PSD curve. There are two parts of PSD analysis, which is hydrometer analysis and mechanical sieving.

Hydrometer analysis is used to determine the fluid density and percentage of finer particles of soil. The reading is taken using hydrometer at specific time. This method is based on Stokes' law (Jury and Horton, 2004), introducing a correlation between particle size and the rate of sedimentation. Particle size can be measured by evaluating the velocity of particles that settle from suspension in a water solution. As soil particles settle, the suspension density decreases. The lower the density of the liquid, the more the hydrometer will sink. The particle size can be



calculated for each measurement time using the observed hydrometer level, and these results are presented in a graph.

Mechanical sieving analysis is necessary for soil classification, especially coarse soils that consist of relative portions of different sizes of particles. It will be possible to determine the percentage of gravel or sand. The remained portions of coarse-grained soil are mechanically sieved in a series of fractions. The results from hydrometer and mechanical sieving analyses will be used to plot the PSD graph. From the relationship on the graph, the percent of a particular particle size class can be estimated (Day, 1965).

## **2.7 X-ray diffraction (XRD) analysis**

Geologic materials such as rocks, sediments, and precipitation are minerals constituted materials. Identification of minerals of these geologic materials is important in the studies of geology, environmental science, material science, engineering, and biology. XRD is fast and efficient in providing accurate information about chemical and physical properties of the sample (Chung, 1975). Majority of the cases, XRD provides an unambiguous mineral determination, and the data interpretation is relatively straight forward. The 3D structure of minerals is characterized as regular, repeating planes of an atom that form a crystal lattice. An interaction of incident rays with minerals samples occurs when an X-ray beam is directed toward the minerals sample. A constructive interference and a diffracted ray are produced when the condition satisfy Bragg's law, givenly Equation 2.7;

$$n\lambda = 2d \sin \theta \quad 2.7$$

where;

$n$  = (an integer) order of diffraction

$\lambda$  = wavelength of the incident X-rays

$d$  = lattice spacing

$\theta$  = angle of incidence

This law refers to the wavelength of electromagnetic radiation to the angle of diffraction and the lattice spacing in a minerals sample. Various diffraction directions of the lattice should be obtained due to the random orientation of the powdered material. Lattice spacing, also known as d-spacing, gives rise to a peak shown in a diffractogram. The identification of the minerals can be done because each mineral has a set of unique d-spacings.

## **2.8 Previous research**

The use of multiple geophysical methods to interpret the subsurface is advantageous because they can complement one another and produce reliable data, thereby improving the subsurface interpretation (Ali et al., 2017; Anuar et al., 2017a; Yusoh et al., 2018). Traditionally, analysis of multiple inversion models derived from separate inversions has been largely limited to visual comparison, in which the inversion images may not benefit mutually. It is not uncommon to discover significant differences between inversion models due to geological heterogeneity and model non-uniqueness (Meju, 1994), owing to the fact that each geophysical method has a different resolution and reflects only one physical property of the underground. Notably, not all of the features of the subsurface structures are supported by both data sets and visible in both inversion images.

Haber and Oldenburg (1997), as well as Zhang and Morgan (1997), proposed a joint inversion method. To perform joint inversion of multiple physical

parameters, a relationship between the physical parameters must be defined in order to connect the inversion models. Gallardo and Meju (2003) incorporating a cross-gradient constraint into the joint inversion method. The structural resemblances between inversion images are related to the distribution of changes in physical properties. These characteristics can be represented mathematically as a vector field of physical property gradients. If the cross-gradient function is equal to zero, the inversion models are structurally similar. Any changes in both physical properties, regardless of their amplitudes, must be in the same or opposite direction.

Numerous papers have been published on cross-gradient joint inversion methods on synthetic models. Gallardo and Meju (2004) used a two-block synthetic model to perform cross-gradient joint inversion of resistivity and seismic data. Through the use of cross-gradient constraint, the resistivity model improved the poorly resolved basal parts and vertical walls of blocks in the seismic model. Hu et al. (2009) conducted joint inversion of conductivity and seismic data on a one-block synthetic model. The block artifacts were smoothed out as a result of a cross-gradient constraint aimed at achieving structural similarity between conductivity and the seismic model. Doetsch et al. (2010) resolved the high resistivity middle layer of three-layer synthetic model by constraining the middle layer with radar and seismic data. Varfinezhad et al. (2020) also demonstrated this method on synthetic model of cavity on top of conductor. The conductor cannot be resolved using resistivity data alone because of a large resistive cavity but can be resolved using magnetic data and a cross-gradient constraint. The poor performance of the resistivity model is attributed to current channeling in the high-conductivity zones, as well as significantly higher sensitivities in the vicinity of the electrodes. Magnetic inversion, on the other hand, does not define the cavity following separate inversion or joint

inversion, as the magnetic method is completely insensitive to it. This demonstrates that cross-gradient constraint will not attempt to create an artificial structure in one geophysical model in order to make it structurally similar to another.

Researchers jointly inverted different geophysical parameters for near-surface investigation. Lochbühler et al. (2013) conducted 3D joint inversion of GPR velocities and hydraulic conductivities data to characterize saturated porous aquifer. Hamdan and Vafidis (2013) delineated saline water zones in karstic geological formations using joint inversion of resistivity and seismic data. Additionally, this study stated that RMS values do not negate the advantages of joint inversion because achieving a unified model is more important during the interpretation process. Massoud et al. (2014) characterized groundwater aquifers using Vertical Electrical Sounding (VES) and Transient Electro-Magnetic (TEM) methods. The joint inversion method overcame model equivalence and layer suppression, resulting in a well-constrained and robust multi-layer model of the subsurface medium. Shi et al. (2017) applied 3D cross-gradient joint inversion of resistivity and seismic data to locate the remains of an ancient city wall. The results show that the inversion model using the joint inversion method are more consistent with the results of the archaeological excavation than those estimated using a single inversion algorithm. Recently, Varfinezhad et al. (2020) performed a joint inversion of resistivity and magnetic data in the Pompeii archaeological area. Joint inversion models are consistent with one another and allow for the more exact identification of subsurface relics from past excavations, whether known or unknown.

Besides that, there are researches on the implementation of joint inversion on similar parameters such as P and S-wave. Tryggvason and Linde (2006) carried out cross-gradient joint inversion to constrain the P and S-wave inversion on a

synthetic model contains of two blocks stacked on top of one another. Boiero and Socco (2014) also conducted joint inversion method to build P and S-wave velocity models to characterize laterally varying layered subsurface. Fu and Liu (2016) manage to detect an unknown buried fault using cross-gradient joint inversion of P-velocity and S-velocity data. Last but not least, Prayitna et al. (2019) used cross-gradient joint inversion of P and S-waves to characterize a landslide.

Many researchers proposed joint inversion of geophysical methods on synthetic models and near-surface investigation to improve the resolution or subsurface characterization of the study area. Implementing the joint inversion method on different types of structures in their study cases is a topic that has received little attention in the literature. Hence, this thesis will focus on integrating joint inversion of 2D resistivity and seismic refraction methods on subsurface with lateral and vertical variation using cross-gradient constraint. The variations in the subsurface included geological structures and man-made structures. This procedure will be carried out using both synthetic models and field data. Additionally, particle size distribution (PSD) and X-ray diffraction (XRD) analyses were performed to aid in classifying the soils and rocks in the study area.

## **2.9 Summary**

This chapter discussed forward modeling, 2D resistivity, seismic refraction, joint inversion with cross gradient constraint, PSD analysis, and XRD analysis. 2D resistivity method and seismic refraction methods are commonly used in subsurface investigation. Forward modeling of resistivity and seismic refraction can be performed prior to study to create a synthetic model that simulates the geological subsurface of a study area. Data processing involving joint inversion with a cross-gradient constraint can be used to build resistivity and seismic models with structural